

Composite microsphere-functionalized scaffold for the controlled release of small molecules in tissue engineering

Journal of Tissue Engineering
Volume 7: 1–11
© The Author(s) 2016
Reprints and permissions:
sagepub.co.uk/journalsPermissions.nav
DOI: 10.1177/2041731415624668
tej.sagepub.com


Laura Pandolfi^{1,2}, Silvia Minardi¹, Francesca Taraballi¹,
Xeuwu Liu¹, Mauro Ferrari¹ and Ennio Tasciotti¹

Abstract

Current tissue engineering strategies focus on restoring damaged tissue architectures using biologically active scaffolds. The ideal scaffold would mimic the extracellular matrix of any tissue of interest, promoting cell proliferation and de novo extracellular matrix deposition. A plethora of techniques have been evaluated to engineer scaffolds for the controlled and targeted release of bioactive molecules to provide a functional structure for tissue growth and remodeling, as well as enhance recruitment and proliferation of autologous cells within the implant. Recently, novel approaches using small molecules, instead of growth factors, have been exploited to regulate tissue regeneration. The use of small synthetic molecules could be very advantageous because of their stability, tunability, and low cost. Herein, we propose a chitosan–gelatin scaffold functionalized with composite microspheres consisting of mesoporous silicon microparticles and poly(DL-lactic-co-glycolic acid) for the controlled release of sphingosine-1-phosphate, a small molecule of interest. We characterized the platform with scanning electron microscopy, Fourier transform infrared spectroscopy, and confocal microscopy. Finally, the biocompatibility of this multiscale system was analyzed by culturing human mesenchymal stem cells onto the scaffold. The presented strategy establishes the basis of a versatile scaffold for the controlled release of small molecules and for culturing mesenchymal stem cells for regenerative medicine applications.

Keywords

Chitosan, gelatin, poly(DL-lactic-co-glycolic acid), silicon, sphingosine-1-phosphate, tissue engineering

Received: 28 October 2015; accepted: 20 November 2015

Introduction

Regenerative medicine aims to restore, maintain, or improve defective tissues by developing biocompatible substitutes.¹ Scaffolds play a pivotal role in tissue engineering as they can be designed to imitate the microarchitecture of native extracellular matrix (ECM) and, therefore, have the potential to promote cell adhesion, growth, and proliferation.² The integration of three-dimensional (3D) pores within the scaffold permit sufficient transport of oxygen, nutrients, metabolites, cellular signals, and regulatory factors.³ This enhances cell survival and proliferation which are instrumental for tissue regeneration.^{4,5} Moreover, these are crucial for scaffold neovascularization.⁶ The ECM of tissues is typically composed of two classes of macromolecules: proteins (e.g. collagen, elastin, and fibrin),⁷ which confer mechanical and bioactive properties to the matrix,⁸

and glycosaminoglycans (e.g. hyaluronic acid, chondroitin sulfate, and heparin sulfate).⁹ In the development of biomimetic materials, several strategies have been proposed to mimic this heterogeneous composition of the ECM using the same² or similar components.¹⁰

¹Department of Nanomedicine, Houston Methodist Research Institute, Houston, TX, USA

²College of Materials Science and Engineering, University of Chinese Academy of Science, Beijing, China

Corresponding author:

Ennio Tasciotti, Department of Nanomedicine, Houston Methodist Research Institute, 6670 Bertner Avenue, Houston, TX 77030, USA.
Email: etasciotti@houstonmethodist.org



Gelatin, a denatured form of collagen type I, has been widely used to mimic the structural protein component of ECM^{11,12} as it contains amino acids that enhance and sustain cell growth and proliferation.¹³ Similarly, chitosan is an extensively utilized glycosaminoglycan; it shares similar molecular structure to those found in most mammalian tissue.¹⁴ Moreover, chitosan has demonstrated to be non-toxic and biocompatible,^{15,16} making it a desirable material for drug delivery^{17,18} and tissue engineering.¹⁹ Chitosan scaffolds are easily fabricated through freeze-drying processes, orienting the pores to favor cell infiltration and new vessel ingrowth.^{20,21} Hence, chitosan and gelatin blends are attractive biomaterials to mimic mammal ECM.²² However, ECM also regulates the spatial presentation of growth factors by binding them to its surface.²³ Control over growth factor release is crucial to trigger specific cell mechanisms and functions necessary for tissue restoration.²⁴ There are various ways to accomplish a biomimetic release of chosen growth factors. In this article, we utilized the physical encapsulation method,²⁵ as an established strategy for the local delivery of bioactive molecules in tissue engineering. Furthermore, this approach helps to minimize factor exposure to harsh conditions *in vivo*, preserving the payload's bioactivity.²⁶

Due to its low toxicity,²⁷ nanostructured silicon multi-stage vectors (MSVs)²⁸ have been extensively used in applications of nanomedicine.^{28–33} Recently, we demonstrated our ability to engineer finely tuned MSV and poly(DL-lactic-co-glycolic acid) (PLGA) composite microspheres (PLGA-MSV) for the spatiotemporal controlled release of proteins *in vivo*.³³ Current approaches to promote and enhance tissue regeneration with scaffolds have mainly focused on growth factor delivery (e.g. vascular endothelial growth factor (VEGF) and transforming growth factor- β (TGF- β)).^{34–36} However, the high cost of growth factors³ and their potential side effects³⁷ drastically limit this strategy. The use of small molecules is an advantageous alternative to growth factors to overcome these limitations³⁸ as they are reliable and easy to manufacture.³⁹

Small molecules' molecular size is also usually too small to induce unwanted immune responses in the host.⁴⁰ Small molecules, extensively used as chemotherapeutic agents for cancer treatment, have although some characteristics that limits their use in clinical applications, including hydrophobicity and nonspecific biodistribution and targeting. To overcome these limitations, the use of a biocompatible platform to localize and sustain the controlled release of small molecules to target sites has been proved to be advantageous.⁴¹ Regenerative engineering utilizing small molecules as pro-regenerative biological factors has been recently emerging.^{42,43} A plethora of small molecules have been studied for tissue-specific adult stem cell targeting (e.g. stemregenin 1,⁴⁴ CASEIN,⁴⁵ and kartogenin⁴⁶). Among all small molecules currently available, sphingosine-1-phosphate (S1P) is of particular interest for tissue regeneration applications because it is a platelet-derived

lipid mediator secreted extensively by platelets in adult mammals and is involved in cell proliferation, migration, and survival.⁴⁷ S1P, when released into the extracellular environment, regulates cell–cell and cell–matrix adhesion, enhancing cell migration and differentiation.^{48,49} S1P has been shown to regulate and control vascular development, vessel stability, and immune cell trafficking. Moreover, it has been proved that S1P promotes recruitment of pericytes and smooth muscle cells supporting the vascular stabilization of newly formed vessels.⁵⁰ The main limitation in engineering *in vitro* tissues is the lack of a sufficient blood vessel system. Therefore, the release of S1P from a tissue engineering implant could be an innovative and advantageous strategy to enhance scaffold's vascularization and boost functional restoration of tissues.

Materials and methods

Preparation and characterization of MSV

Discoidal MSV particles of 1 μm in diameter and 400 nm thicknesses were fabricated by photolithography and electrochemical porosification of patterned silicon wafers as extensively described elsewhere.⁵¹ MSVs were then oxidized⁵² and lyophilized. Lyophilized particles were suspended in distilled water and 20 μL deposited on specific metal stands for further analysis. Samples were coated with 3 nm of Pt/Pb and scanning electron microscopy (SEM) (FEI Quanta 400 ESEM FEG; FEI, Hillsboro, OR, USA) imaging analysis performed at 7 kV to evaluate their morphology.

Preparation and characterization of PLGA

A modified double-emulsion technique was adopted to prepare S1P-loaded PLGA (LACTEL, Cupertino, CA, USA) microspheres. The inherent copolymer viscosity was 0.55–0.75 dL g^{-1} .

PLGA copolymer ratio was set to 50:50; PLGA was dissolved in dichloromethane (DCM) (Sigma–Aldrich, St Louis, MO, USA) at a concentration of 50 mg mL^{-1} (5% w/v). 2 mL of PLGA solution in DCM with a total of 300 $\mu\text{g mL}^{-1}$ of S1P were stirred with poly(vinyl alcohol) (PVA) (Fisher Scientific; Pittsburgh, PA, USA) 2.5% (w/v) for 10 min at 3500 r/min using a homogenizer. This emulsion was then dropped into 40 mL of PVA 1% (w/v) solution. The microspheres were hardened with vigorous stirring for 4 h, washed three times with distilled water, and collected by centrifugation. The microspheres were subsequently lyophilized and stored under vacuum until further use. SEM analysis was performed to investigate shape and size of PLGA microparticles.

Preparation and characterization of PLGA-MSV

After lyophilization, MSVs were encapsulated in PLGA microparticles via a modified double-emulsion method as

previously described.³³ PLGA copolymer ratio was set to 50:50 and the PLGA was dissolved in DCM at a concentration of 5% (w/v). 2×10^8 dried MSVs were emulsified with 1 mL of PLGA 5% (w/v) and 3 mL of PVA 2.5% (w/v) at 3500 r/min for 10 min. The emulsion was then dropped into 40 mL of PVA 1% (w/v). The final solution was stirred for 4 h to allow DCM to evaporate. Particles were then washed three times with distilled water, collected by centrifugation, and subsequently lyophilized. Full encapsulation of MSV microparticles in PLGA microspheres was assessed by optical microscopy. The NIH software ImageJ (NIH Image, Bethesda, MD, USA) was used to measure microsphere diameters and investigate shape and size of PLGA-MSV composites.

Loading of reporter molecule fluorescein isothiocyanate and S1P into PLGA-MSV particles

In order to load the selected reporter molecule, 2×10^8 MSVs were suspended in 500 μ L of fluorescein isothiocyanate (FITC) solution (Sigma–Aldrich) in distilled water (10 mg mL⁻¹), followed by 2 h of incubation in physiological-like conditions (37°C, under mild agitation). Centrifugation at 4500 r/min for 10 min allowed for particle isolation. The collected supernatant was used to estimate the amount of absorbed reporter molecules by mass difference, using a spectrophotometer (SpectraMax M2; Molecular Devices, Sunnyvale, CA, USA), at $\lambda=495$ nm/555 nm. The FITC-loaded particles were then lyophilized overnight and subsequently encapsulated in a 5% 50:50 PLGA shell, as described above. Following the same procedure, S1P (TOCRIS, Bristol, UK) was loaded into PLGA-MSV microspheres at a concentration of 300 μ g mL⁻¹. An enzyme-linked immunosorbent assay (ELISA) kit (ECHELON, Salt Lake City, UT, USA) was used to quantify S1P concentration in the microspheres and samples. We measured the absorbance at 450 nm and determined the S1P concentration in the collected supernatants using a standard curve.

Scaffold fabrication

Porous chitosan–gelatin (CHI:GEL) scaffolds, 2 mm in height and 9 mm in diameter, were produced by freeze-drying method using a 48-well plate as a mold. A 2% (w/v) solution of chitosan (Sigma–Aldrich) in 0.5 M acetic acid was prepared by dissolving the required amount of chitosan in the solvent and stirring for 2 h to get a fully transparent solution. A 1% (w/v) solution of gelatin (Sigma–Aldrich) in deionized water (di-H₂O) was prepared by dissolving the required amount of gelatin in di-H₂O and stirring for 2 h. The two solutions were then mixed at the desired ratio (1:1) and emulsified through sonication for 30 min at room temperature. One-third of the slurry was enriched with 30 mg of S1P-loaded PLGA-MSV particles

(CHI:GEL/PLGA-MSV), one-third of the slurry was functionalized with PLGA microspheres containing S1P (CHI:GEL/PLGA), and the remaining slurry was used to obtain blank scaffolds and reporter scaffolds with FITC-loaded PLGA-MSV (CHI:GEL/FITC). To obtain the scaffolds, 500 μ L of each solution were put in a 48-well plate and frozen at -80°C for 4 h, and subsequently lyophilized overnight. CHI:GEL without microparticles (CHI:GEL blank) were used as controls for in vitro studies. Samples were then coated with 5 nm of Pt/Pb and SEM analysis was performed at 7 kV to evaluate their microarchitecture.

Scaffold crosslinking

Once lyophilized, all scaffolds were crosslinked using a 1-ethyl-3-(3-dimethylaminopropyl)-carbodiimide/N-hydroxysuccinimide (EDC/NHS) coupling method to enhance their mechanical properties and stability in physiological-like conditions. Briefly, lyophilized scaffolds were soaked in 1 mL of ethanol/water (9:1, v/v) solution containing 75 mM of EDC (Sigma–Aldrich) and 30 mM of NHS (Sigma–Aldrich) for 24 h at 4°C. The molar ratio of EDC/NHS was constant to 5:2. After crosslinking, unbound and excess EDC and NHS were removed by washing the implants with phosphate-buffered saline (PBS) three times. The scaffolds were frozen at -30°C for 4 h and then freeze-dried overnight under vacuum.

Scaffold swelling

In order to evaluate the ability of the scaffolds to uptake PBS, the lyophilized implants were weighed (W_d) and incubated in physiological-like condition up to 7 days. The hydrated scaffolds were taken out of the PBS at different time points and hung up until no dripping water was observed and then weighed again (W_h). The percentage of absorbed PBS within the scaffold, defined as swelling, was calculated using the following equation

$$\text{Absorbed PBS}(\%) = \frac{(W_h - W_d)}{W_d} \times 100$$

Fourier transform infrared characterization

Fourier transform infrared (FTIR) spectroscopy was performed by creating a pellet of sample and KBr (Sigma–Aldrich) (5% and 95%, by volume, respectively) and analyzing absorbance of the pellet on a Nicolet 6700 FTIR Spectrometer (ThermoFisher Scientific Inc., Waltham, MA, USA). The spectra were reported after background subtraction, baseline correction, and binomial smoothing (11 points) using OMNIC software (ThermoFisher Scientific Inc.).

Cell seeding on CHI:GEL

Early passage human mesenchymal stem cells (hMSC), supplied by the Institute for Regenerative Medicine, Texas A&M Health Science Center, were seeded onto the scaffolds at a density of 100,000 cells cm^{-2} . The scaffolds, after sterilization for 24 h under ultraviolet (UV) light, were seeded with hMSC. Cells had been grown for a total of 7 days. The culture medium contained 87% alpha minimum essential medium (MEM) with 10% heat inactivated serum (fetal bovine serum (FBS)), 2% glutamine, and 1% PenStrep (v/v). The cells were also supplemented with 1% (v/v) basic fibroblast growth factor (bFGF) solution. To measure cell proliferation, the seeded scaffolds and control wells were incubated for 3 h with fresh culture medium supplemented with 10% (v/v) alamarBlue[®]. Three replicates were used for each group of scaffolds. Following incubation, 100 μL of medium from each well was transferred, in triplicate, to a 96-well microplate. Absorbance measurements were taken every day, throughout the experiment, using a spectrophotometer SpectraMax M2 at $\lambda = 570 \text{ nm}$, using 600 nm as a reference wavelength.

Cell viability assay

Scaffolds seeded with hMSC were removed from their original culture wells and washed with PBS for 5 min. Following this washing step, samples were stained for a Live/Dead Viability/Cytotoxicity assay (Molecular Probes, Eugene, OR, USA) according to the manufacturer's protocol. The samples were then visualized immediately using confocal laser microscopy imaging (A1 Nikon Confocal Microscope; Nikon Instruments Inc., Melville, NY, USA).

Evaluation of hMSC morphology

Each group of scaffolds (CHI:GEL blank and CHI:GEL/PLGA-MSV, respectively), at 24 h and 7 days, were analyzed by confocal laser microscopy and SEM. Cell arrangement in the scaffolds was evaluated by confocal laser microscopy (Nikon Instruments Inc.), by staining the nuclei with 4',6-diamidino-2-phenylindole (DAPI) (ThermoFisher Scientific Inc.) and actin filaments with phalloidin (ThermoFisher Scientific Inc.), according to manufacturer instructions. 3D renderings were obtained by the NIS-Element software (Nikon Instruments Inc.). After 7 days of culture, one sample was fixed and dehydrated for SEM imaging, following the standard protocol for preparation described previously.³³ Samples were sputter coated with 5 nm of Pt/Pb and imaged at 10 kV to evaluate cell morphology.

Statistics

Statistics for experiments were performed using a two-way analysis of variance (ANOVA) followed by Tukey's multiple

comparison test. A p-value of <0.05 was considered significant. All experiments were performed, at minimum, in triplicate. Data are presented as mean \pm standard deviation (SD).

Results and discussion

PLGA-MSV characterization

Controlling the shape and size of the delivery system is of principal importance to control the system loading efficiency and desired release kinetics. Discoidal MSV particles (Figure 1(a)) with a diameter of 1 μm and a total porosity of 51% were produced through an optimized, scalable, and reproducible lithographic method, providing batches of uniform MSV.⁵¹ We used a modified double-emulsion method³³ to create the composite microspheres and encapsulate MSV in the PLGA microspheres (Figure 1(b)). According to results previously published about the influence of the composite microsphere's outer shell on the loaded molecule's release kinetics, 50:50 PLGA with a viscosity of 0.55–0.75 dLg^{-1} was chosen for our studies to obtain a total release of SIP within 2 weeks.³³ The encapsulation of MSV in PLGA was assessed by optical microscopy (Figure 1(c)), allowing us to verify the embedding and amount of MSV within each micro-particle. Moreover, SEM images of the final delivery platforms were taken and analyzed with ImageJ (Figure 1(d)). The majority of the produced PLGA-MSV microcomposites showed an average diameter of $2.52 \pm 1.49 \mu\text{m}$ (Figure 1(e)).

Characterization of the scaffolds

CHI:GEL in lyophilized and hydrated states are shown in Figure 2(a) and (b), respectively. SEM analysis was performed to determine scaffold microstructures; micrographs of CHI:GEL blank (Figure 2) and CHI:GEL/PLGA-MSV (Figure 3) display an interconnected porous structure, with an overall anisotropic and interconnected porosity of 60%–70% of the total volume determined using ImageJ. Both scaffolds showed pore sizes between 50 and 150 μm , providing an ideal environment for attachment and growth of cells.⁵³ The porosity and wall thickness of the surface (Figure 2(a) and (d)) and cross-section (Figure 2(e) and (f)) of CHI:GEL blank present the same morphology, proving the homogeneity of the platform. Similarly, from the SEM micrographs of CHI:GEL/PLGA-MSV surface (Figure 3(a) and (b)) and CHI:GEL/PLGA-MSV cross-section (Figure 3(c) and (d)), we can conclude that they exhibit similar microstructure. Moreover, the addition of PLGA-MSV to the scaffold did not affect the microarchitecture of CHI:GEL/PLGA-MSV. These results confirmed that PLGA-MSV microspheres added to the chitosan–gelatin solution at the slurry state were fully integrated in the scaffold and did not affect the final microarchitecture of the platform. This correlates with the previous findings of Minardi et al.,³² in which PLGA-MSV were integrated into a 3D collagen type I scaffold.

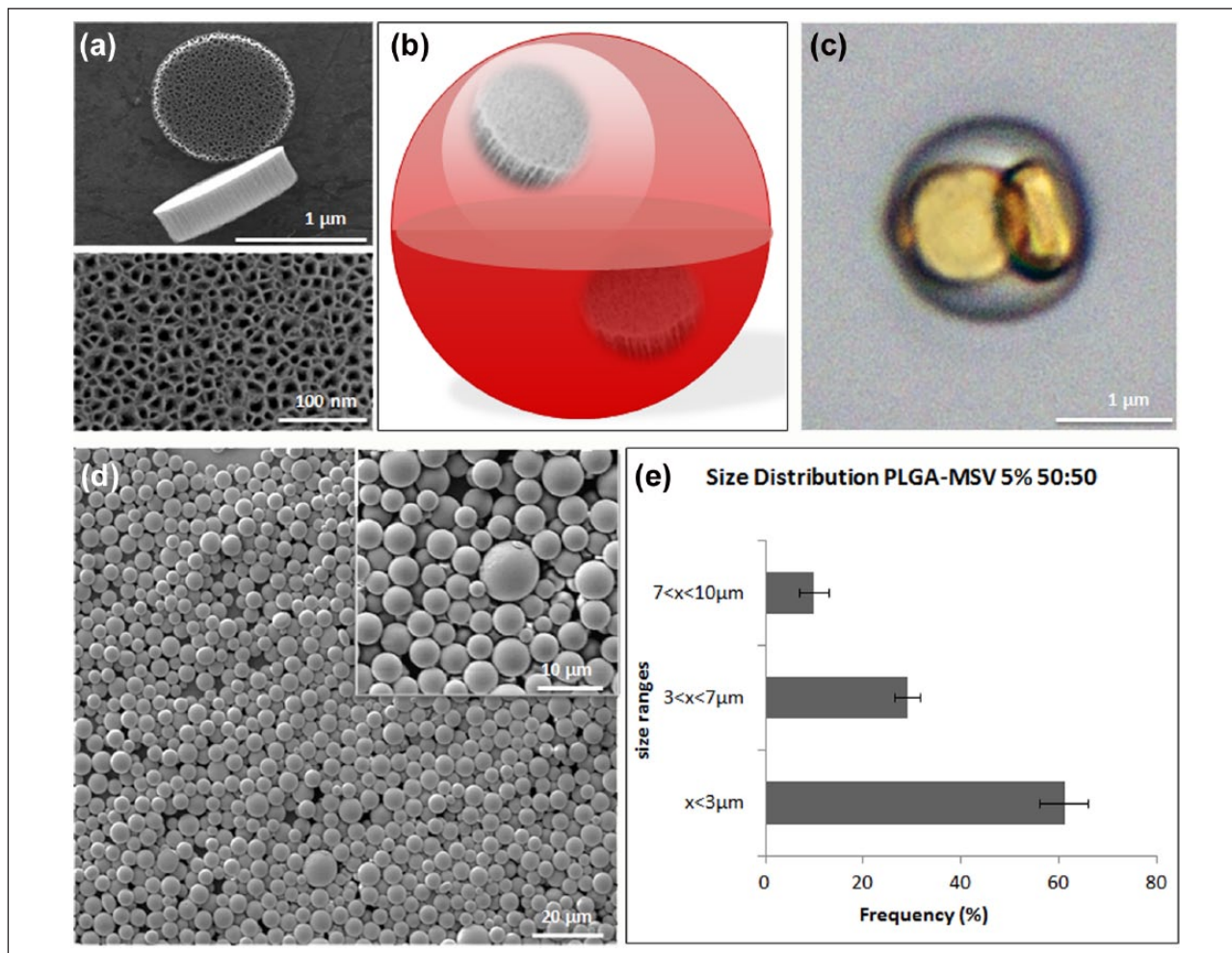


Figure 1. (a) SEM images of individual discoidal MSV (top), including the close-up view of its pores (bottom). (b) Schematic diagram of the MSV encapsulated in PLGA microspheres. (c) Optical microscope image of MSV-PLGA composite microspheres (PLGA: transparent sphere; MSV: brownish disks). (d) SEM images of PLGA-MSV microspheres illustrating their typical shape and uniformity, including a close-up view of the delivery platform in the inset. (e) Size distribution of PLGA-MSV (5% 50:50, 1 μm)

The mean distance between PLGA-MSV microspheres integrated in the scaffold was calculated in 20 random positions and found to be $15.3 \pm 2.1 \mu\text{m}$. Swelling properties of the scaffolds were not affected by the integration of PLGA-MSV microparticles, as shown in Figure 3(e). FTIR was performed to confirm the chemical composition of the scaffolds and PLGA-MSV microparticles, as can be seen in Figure 3(f). The spectroscopic analysis of the CHI:GEL confirmed the presence of a blend of the two structural macromolecules. The carbohydrate moieties (CHI) around 1000 cm^{-1} arise from the gelatin protein structure; the PLGA-MSV moieties are hidden by the bulk structure of the scaffold.

In vitro release of FITC and S1P

Several sets of delivery systems were created to evaluate the release kinetics from both the delivery system and the CHI:GEL. S1P was loaded into PLGA microspheres (5%

50:50) and PLGA-MSV (1 μm , 5% 50:50) microparticles for *in vitro* release. The assessed loading efficiency of S1P was $24.1\% \pm 3.3\%$ in PLGA microspheres and $62.2\% \pm 5.7\%$ in the PLGA-MSV. As expected from previously published work,³³ the loading efficiency within the PLGA-MSV microparticles was demonstrated to increase 40% compared to that of PLGA particles alone.

Release profiles for all groups were performed in physiological-like conditions for up to 10 days. As a proof of concept, the CHI:GEL/FITC was tested to visualize how small molecules release and diffuse within the 3D scaffold. We could see that FITC diffused homogeneously and radially from the microspheres at different time points (Figure 4(a)–(g)) because PLGA-MSV particles are homogeneously sized and distributed within the scaffold. The results obtained with FITC were particularly informative because of its similar molecular weight to S1P (389.4 and 379.5 Da, respectively). The cumulative release profile of FITC is shown in Figure 4(g). The obtained FITC release kinetics

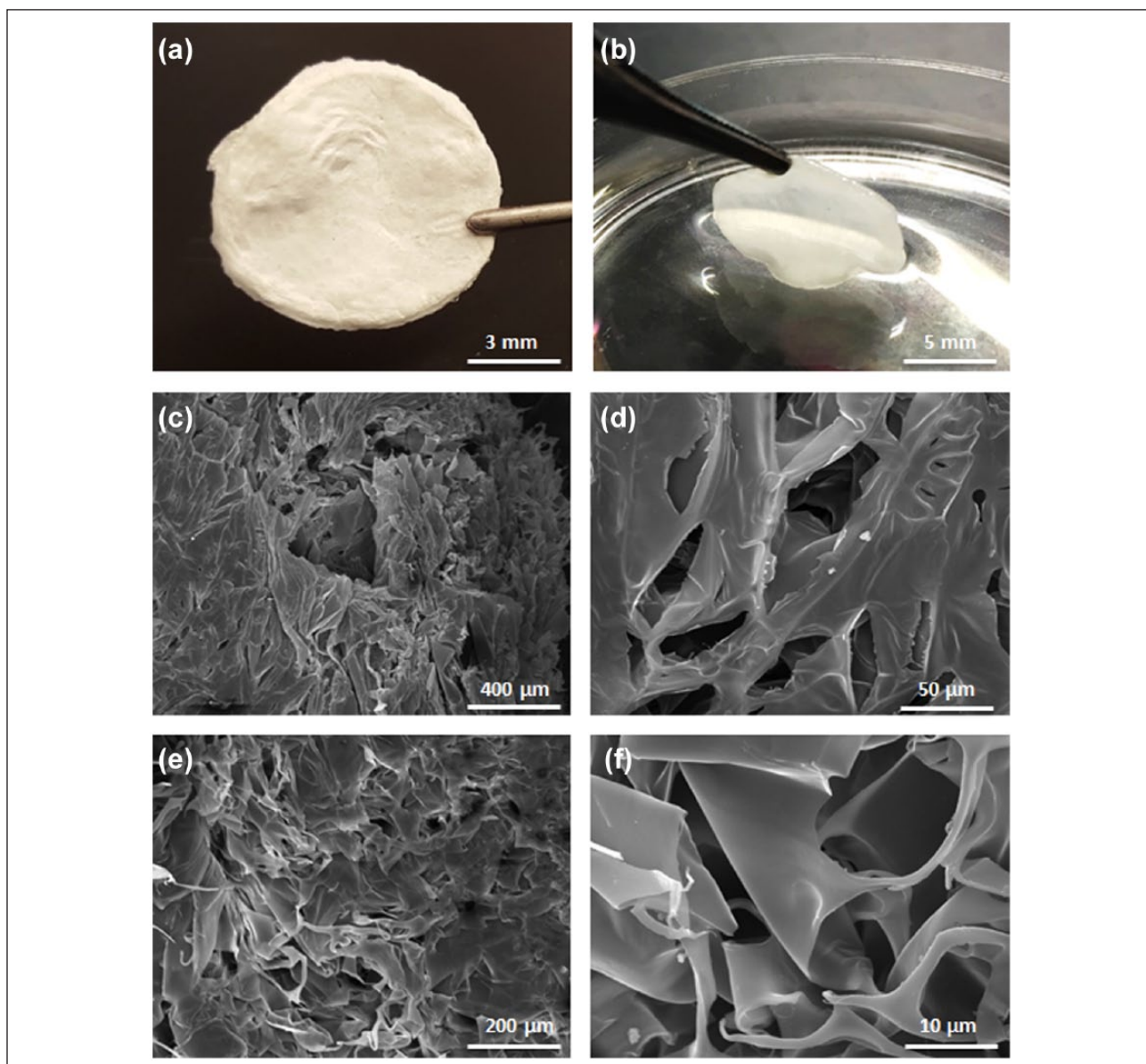


Figure 2. (a) Lyophilized CHI:GEL. (b) Hydrated CHI:GEL. (c, d) SEM images of CHI:GEL blank surface. (e, f) CHI:GEL blank cross-section.

match the release profile of S1P from CHI:GEL/PLGA-MSV (Figure 4(h)).

As previously reported,^{51,54} release from PLGA microparticles (5% 50:50) occurred at faster rates with an evident burst release compared to the slower kinetics obtained with PLGA-MSV composite microparticles. PLGA microparticles released almost 80% of their payload within the first 48 h. Moreover, it is possible to see how all three components of the functionalized scaffold (MSV, PLGA, and CHI:GEL) contributed to steady controlled release up to 10 days. The controlled release of molecules over long periods of time is crucial to favor on-platform regeneration and reduce side effects caused by overdosing the surrounding tissue.²⁹

In vitro cell viability and proliferation

The behavior of hMSC cultured on CHI:GEL was assessed to determine whether changing the surface micro-topography of the material affected their viability and proliferation *in vitro* over 7 days; viability was assessed by LIVE/DEAD[®] assay. As shown in Figure 5(a), hMSC displayed high viability on CHI:GEL/PLGA-MSV after 3 days. Cells in the scaffolds grew in a similar fashion to the controls, although proliferation of hMSC on the scaffolds was generally slower than control cells (Figure 5(b)), matching with previous studies.⁵⁵ Confocal laser microscopy was used to acquire Z-stacks and reconstruct the 3D structure of the scaffolds (white) (Figure 5(c) and (d)).

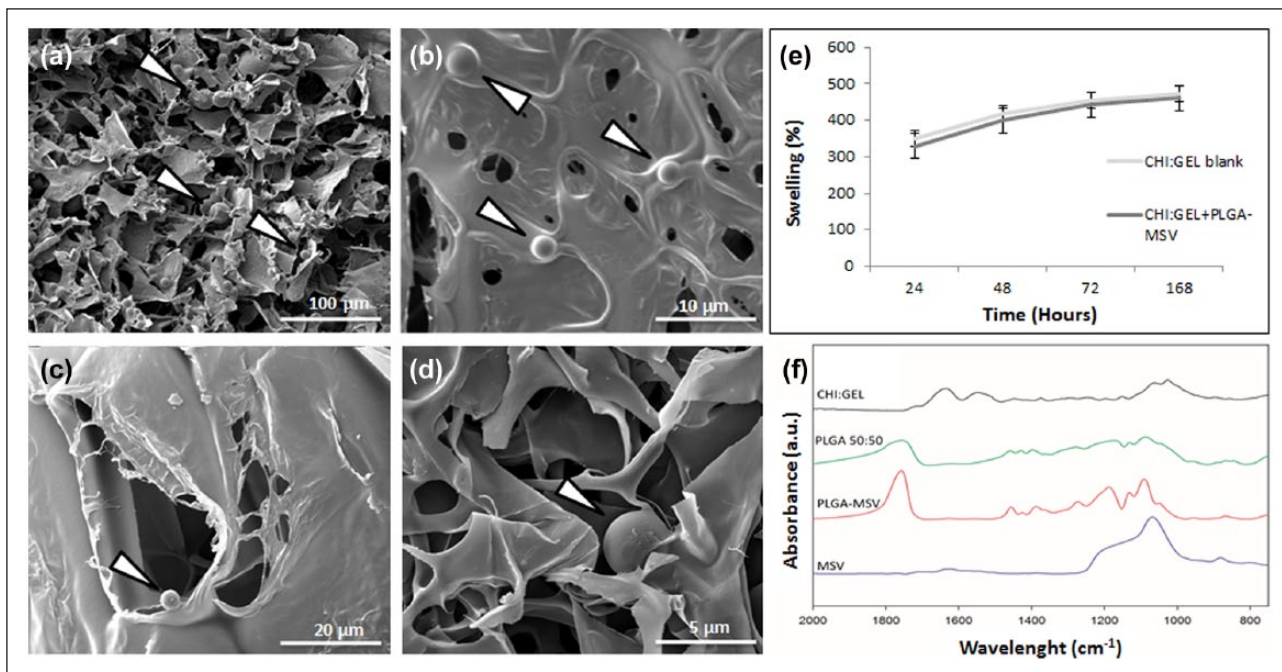


Figure 3. (a, b) SEM images of the surface and (c, d) cross-section of CHI:GEL functionalized with PLGA-MSV microspheres. The microspheres, indicated by white arrows, result perfectly integrated in the scaffold structure. (e) Swelling characteristics comparing CHI:GEL blank and CHI:GEL/PLGA-MSV. (f) FTIR patterns of the components of the multiscale scaffold.

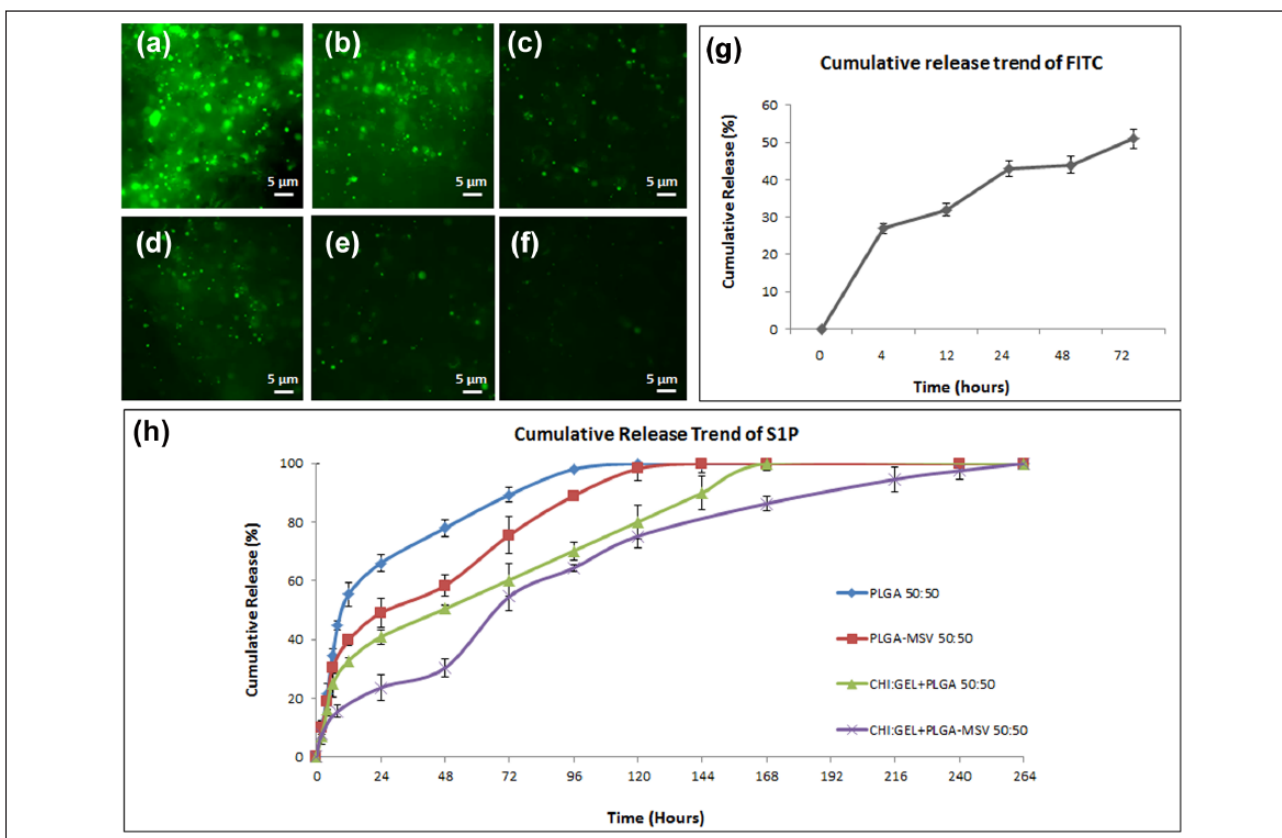


Figure 4. Release profiles. (a)–(f) 3D release of FITC from CHI:GEL/PLGA-MSV. (g) Cumulative release of FITC from CHI:GEL/PLGA-MSV. (h) Overall results of all the 2D and 3D platforms investigated for S1P release.

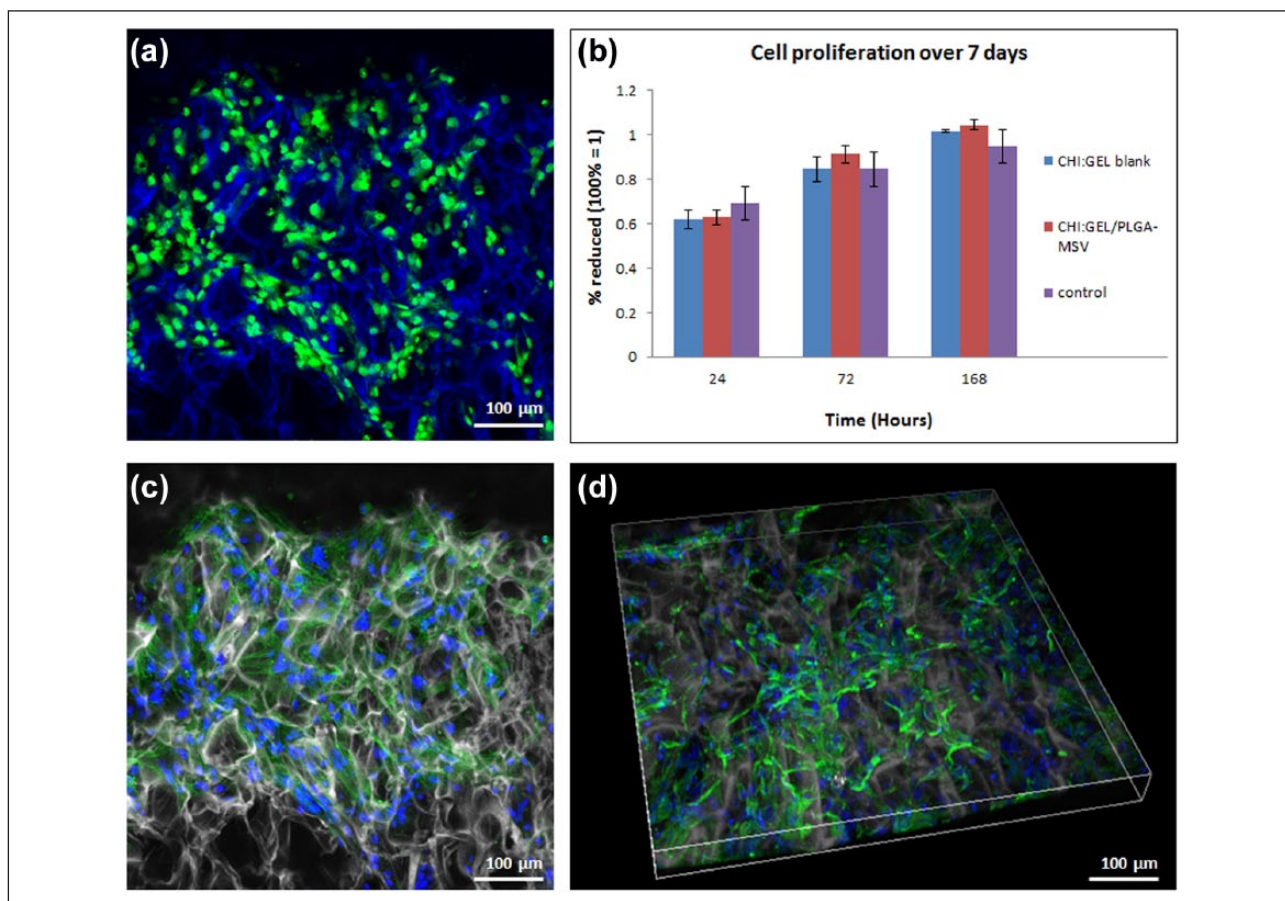


Figure 5. Cell morphology analysis by immunofluorescence and 3D reconstruction of confocal microscopy images. (a) Fluorescence microscopy images of cells stained with LIVE/DEAD[®] at 72 h. (b) Cell proliferation results over 7 days. (c) Confocal laser micrographs of hMSC on CHI:GEL/PLGA-MSV at 7 days. (d) 3D rendering illustrating the morphology of the scaffold and the distribution of hMSC within the structure. Phalloidin in green stains for actin filaments and DAPI in blue stains for cell nuclei.

Using the 3D rendering, we found the pore sizes of CHI:GEL to be in the range of 50–150 μm , confirming the results obtained previously with ImageJ.

The typical fusiform shape of hMSC was retained on CHI:GEL and appeared homogeneously spread in the pores of the material.⁵⁶ Furthermore, SEM micrographs displayed that the type of scaffold surface—CHI:GEL blank (Figure 6(a) and (b)) or CHI:GEL/PLGA-MSV (Figure 6(c) and (d))—did not influence the degree of cell adhesion. It is well known that material's composition and porosity can affect cell adhesion and phenotype.^{57,58} Cells eventually adhere to a compatible material, involving a series of physicochemical linkages between the cells and the material.⁵⁹ Cell spreading is an essential function of a cell adherence to a material surface and is paramount for cell proliferation.⁶⁰ At day 7, the degradation of PLGA-MSV integrated within the scaffold resulted in collapsed doughnut-shaped or toroid-shaped microparticles, as we can see from Figure 6(c) and (d). This might be because the particles did not support the scaffold's layer once they started to degrade, supporting our hypothesis about the complete integration of PLGA-MSV in the scaffold walls.

Conclusion

The combination of drug delivery systems with tissue engineering platforms has shown to be a promising approach for regenerative medicine applications. Nevertheless, delivery platforms have a series of shortcomings, mostly related to their inability to precisely control the release of their payloads, resulting in disruptive side effects for patients and limiting their translation to the clinic. The controlled release of small molecules can be used to reduce the amount of drug necessary to obtain the same therapeutic effect. Many types of biomaterials, from biologically derived ones to those of synthetic origin, have been engineered to address this need; biocompatible and biodegradable platforms are of the utmost interest. Herein, we showed that a biocompatible scaffold functionalized with PLGA-MSV allowed for the controlled release of S1P. S1P, the molecule of interest, has been shown to have a pivotal role in some crucial processes in the regenerative cascade: extracellularly it regulates cell migration and intracellularly enhances cell survival and proliferation. Sustained release from ceramic and polymeric carriers has been previously proposed as a viable strategy

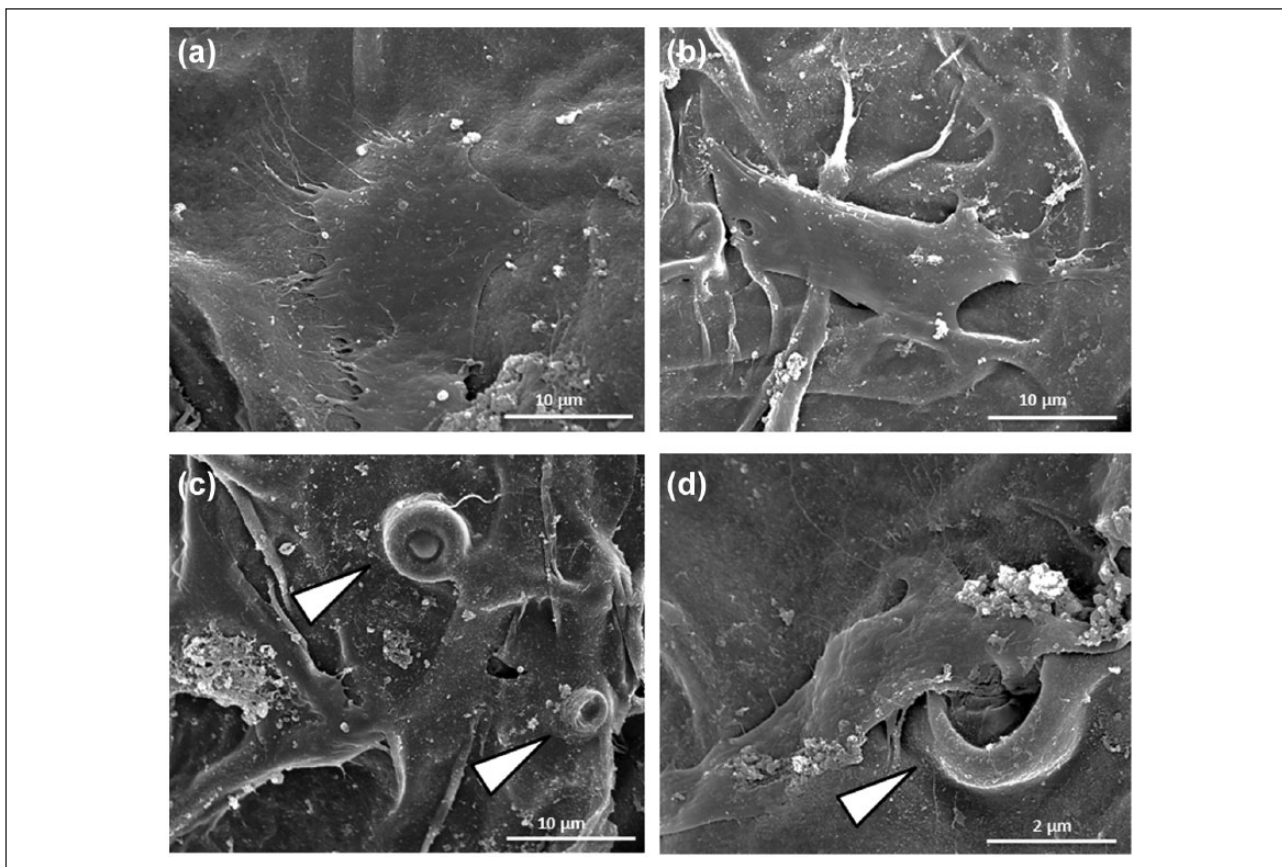


Figure 6. SEM micrographs of scaffolds seeded with hMSC. (a, b) CHI:GEL blank seeded with hMSC at 7 days. (c, d) CHI:GEL functionalized with PLGA-MSV seeded with hMSC at day 7.

for small molecule drugs; however, the main problem with using these carriers as delivery systems is the difficulty in controlling sustained delivery rates. This is particularly true for low-molecular-weight drugs because the diffusion rate is faster and the initial burst release cannot be prevented.

The herein presented platform strategy is a novel approach to establish the basis of a versatile scaffold for the controlled release of small molecules to overcome the lack of standard and effective delivery of small molecules. Our approach holds promise as an alternative strategy to growth factor release with the aim of inducing tissue restoration for a plethora of clinical applications. Further investigations are necessary to verify the efficacy of this platform in vivo.

Acknowledgements

The authors acknowledge Ms Nupur Basu for harvesting the cells used in this study. They would also like to thank Ms Megan Livingston and Ms Kelly Hartman for their help in editing this publication. They thank Dr J Gu of the HMRI Microscopy-SEM/AFM core.

Declaration of Conflicting Interests

The author(s) declared no potential conflicts of interest with respect to the research, authorship, and/or publication of this article.

Funding

The author(s) disclosed receipt of the following financial support for the research, authorship, and/or publication of this article: This study was financially supported by the following sources: Department of Defense grants W81XWH-09-1-0212 and W81XWH-12-1-0414, National Institute of Health grants U54CA143837 and U54CA151668, the CPRIT grant RP121071 from the State of Texas, and the Ernest Cockrell Jr Distinguished Endowed Chair. This study was also supported by the Brown Foundation (Project ID: 18130011) and by the Cullen Trust for Health Care Foundation (Project ID: 18130014).

References

1. Karp JM and Langer R. Development and therapeutic applications of advanced biomaterials. *Curr Opin Biotechnol* 2007; 18: 454–459.
2. Geckil H, Xu F, Zhang X, et al. Engineering hydrogels as extracellular matrix mimics. *Nanomedicine* 2010; 5: 469–484.
3. Lovett M, Lee K, Edwards A, et al. Vascularization strategies for tissue engineering. *Tissue Eng Part B Rev* 2009; 15: 353–370.
4. Annabi N, Nichol JW, Zhong X, et al. Controlling the porosity and microarchitecture of hydrogels for tissue engineering. *Tissue Eng Part B Rev* 2010; 16: 371–383.

5. Sant S, Hancock MJ, Donnelly JP, et al. Biomimetic gradient hydrogels for tissue engineering. *Can J Chem Eng* 2010; 88: 899–911.
6. Nomi M, Atala A, De Coppi P, et al. Principals of neovascularization for tissue engineering. *Mol Aspects Med* 2002; 23: 463–483.
7. Barker TH. The role of ECM proteins and protein fragments in guiding cell behavior in regenerative medicine. *Biomaterials* 2011; 32: 4211–4214.
8. Alberts B, Johnson A, Lewis J, et al. Chapter 19. Cell junctions, cell adhesion and the extracellular matrix. In: Alberts B, Johnson A, Lewis J, et al. (eds) *Molecular biology of the cell*. New York: Garland Science, 2002, pp. 1090–1124.
9. Divya P and Krishnan LK. Glycosaminoglycans restrained in a fibrin matrix improve ECM remodelling by endothelial cells grown for vascular tissue engineering. *J Tissue Eng Regen Med* 2009; 3: 377–388.
10. Tibbitt MW and Anseth KS. Hydrogels as extracellular matrix mimics for 3D cell culture. *Biotechnol Bioeng* 2009; 103: 655–663.
11. Dubruel P, Schacht E, Van Vlierberghe S, et al. Gelatin as promising cell-interactive ECM mimicking biomaterial. In: *Proceedings of the 4th congress on regenerative biology and medicine*, Stuttgart, 13–15 October 2011, pp. 545–545. Ghent: Ghent University Academic Bibliography.
12. Lei B, Shin K-H, Noh D-Y, et al. Nanofibrous gelatin–silica hybrid scaffolds mimicking the native extracellular matrix (ECM) using thermally induced phase separation. *J Mater Chem* 2012; 22: 14133–14140.
13. Zhang Z, Li G and Shi B. Physicochemical properties of collagen, gelatin and collagen hydrolysate derived from bovine limed split wastes. *J Soc Leath Tech Ch* 2006; 90: 23.
14. Ma PX and Elisseeff J. *Scaffolding in tissue engineering*. Boca Raton, FL: CRC Press, 2005.
15. Thanou M, Verhoef J and Junginger H. Oral drug absorption enhancement by chitosan and its derivatives. *Adv Drug Deliv Rev* 2001; 52: 117–126.
16. Semwal A, Singh R and Dutta P. Chitosan: a promising substrate for pharmaceuticals. *J Chitin Chitosan Sci* 2013; 1: 87–102.
17. Felt O, Buri P and Gurny R. Chitosan: a unique polysaccharide for drug delivery. *Drug Dev Ind Pharm* 1998; 24: 979–993.
18. Taraballi F, Minardi S, Corradetti B, et al. Potential avoidance of adverse analgesic effects using a biologically “Smart” hydrogel capable of controlled bupivacaine release. *J Pharm Sci* 2014; 103: 3724–3732.
19. Hussain A, Collins G and Cho CH. Electrospun chitosan-based nanofiber scaffolds for cardiac tissue engineering applications. In: *Proceedings of the 2010 IEEE 36th annual northeast bioengineering conference*, New York, 26–28 March 2010, pp. 1–2. New York: IEEE.
20. Jana S, Florczyk SJ, Leung M, et al. High-strength pristine porous chitosan scaffolds for tissue engineering. *J Mater Chem* 2012; 22: 6291–6299.
21. Muehleder S, Ovsianikov A, Zipperle J, et al. Connections matter: channeled hydrogels to improve vascularization. *Front Bioeng Biotechnol* 2014; 2: 52.
22. Huang Y, Onyeri S, Siewe M, et al. In vitro characterization of chitosan–gelatin scaffolds for tissue engineering. *Biomaterials* 2005; 26: 7616–7627.
23. Schultz GS and Wysocki A. Interactions between extracellular matrix and growth factors in wound healing. *Wound Repair Regen* 2009; 17: 153–162.
24. Chen F-M, Zhang M and Wu Z-F. Toward delivery of multiple growth factors in tissue engineering. *Biomaterials* 2010; 31: 6279–6308.
25. Lee K, Silva EA and Mooney DJ. Growth factor delivery-based tissue engineering: general approaches and a review of recent developments. *J R Soc Interface* 2011; 8: 153–170.
26. Yuan W and Liu Z. Controlled-release and preserved bioactivity of proteins from (self-assembled) core-shell double-walled microspheres. *Int J Nanomedicine* 2012; 7: 257.
27. Fan D, De Rosa E, Murphy MB, et al. Mesoporous silicon-PLGA composite microspheres for the double controlled release of biomolecules for orthopedic tissue engineering. *Adv Funct Mater* 2012; 22: 282–293.
28. Godin B, Tasciotti E, Liu X, et al. Multistage nanovectors: from concept to novel imaging contrast agents and therapeutics. *Acc Chem Res* 2011; 44: 979–989.
29. Wolfram J, Shen H and Ferrari M. Multistage vector (MSV) therapeutics. *J Control Release* 2015; 219: 406–415.
30. Sakamoto J, Annapragada A, Decuzzi P, et al. Antibiological barrier nanovector technology for cancer applications. *Expert Opin Drug Deliv* 2007; 4: 359–369.
31. Shen H, Sun T and Ferrari M. Nanovector delivery of siRNA for cancer therapy. *Cancer Gene Ther* 2012; 19: 367–373.
32. Minardi S, Sandri M, Martinez JO, et al. Multiscale patterning of a biomimetic scaffold integrated with composite microspheres. *Small* 2014; 10: 3943–3953.
33. Minardi S, Pandolfi L, Taraballi F, et al. PLGA-mesoporous silicon microspheres for the in vivo controlled temporospatial delivery of proteins. *ACS Appl Mater Interfaces* 2015; 7: 16364–16373.
34. Ekaputra AK, Prestwich GD, Cool SM, et al. The three-dimensional vascularization of growth factor-releasing hybrid scaffold of poly (ϵ -caprolactone)/collagen fibers and hyaluronic acid hydrogel. *Biomaterials* 2011; 32: 8108–8117.
35. Ferrara N, Houck K, Jakeman L, et al. Molecular and biological properties of the vascular endothelial growth factor family of proteins. *Endocr Rev* 1992; 13: 18–32.
36. Tomanek RJ, Lotun K, Clark EB, et al. VEGF and bFGF stimulate myocardial vascularization in embryonic chick. *Am J Physiol* 1998; 274: H1620–H1626.
37. Schaper W, Piek J, Munoz-Chapuli R, et al. Collateral circulation of the heart. In: Ware JA and Simons M (eds) *Angiogenesis and cardiovascular disease*. New York: Oxford University Press, 1999, pp. 159–198.
38. Kramer T, Schmidt B and Lo Monte F. Small-molecule inhibitors of GSK-3: structural insights and their application to Alzheimer’s disease models. *Int J Alzheimer Dis* 2012; 2012: 381029.
39. Emre N, Coleman R and Ding S. A chemical approach to stem cell biology. *Curr Opin Chem Biol* 2007; 11: 252–258.
40. Blaich G, Janssen B, Roth G, et al. Overview: differentiating issues in the development of macromolecules compared with small molecules. In: Cad SX (ed.) *Pharmaceutical sciences encyclopedia*. New York: John Wiley & Sons, 2010, pp. 89–123.

41. Chen Z. Small-molecule delivery by nanoparticles for anti-cancer therapy. *Trends Mol Med* 2010; 16: 594–602.
42. Laurencin CT, Ashe KM, Henry N, et al. Delivery of small molecules for bone regenerative engineering: preclinical studies and potential clinical applications. *Drug Discov Today* 2014; 19: 794–800.
43. Lo KW, Ashe KM, Kan HM, et al. The role of small molecules in musculoskeletal regeneration. *Regen Med* 2012; 7: 535–549.
44. Thordardottir S, Hangalapura BN, Hutten T, et al. The aryl hydrocarbon receptor antagonist StemRegenin 1 promotes human plasmacytoid and myeloid dendritic cell development from CD34+ hematopoietic progenitor cells. *Stem Cells Dev* 2013; 23: 955–967.
45. Shang X, Marchioni F, Sipes N, et al. Rational design of small molecule inhibitors targeting RhoA subfamily Rho GTPases. *Chem Biol* 2012; 19: 699–710.
46. Johnson K, Zhu S, Tremblay MS, et al. A stem cell-based approach to cartilage repair. *Science* 2012; 336: 717–721.
47. Maceyka M, Harikumar KB, Milstien S, et al. Sphingosine-1-phosphate signaling and its role in disease. *Trends Cell Biol* 2012; 22: 50–60.
48. Blaho VA and Hla T. Regulation of mammalian physiology, development, and disease by the sphingosine 1-phosphate and lysophosphatidic acid receptors. *Chem Rev* 2011; 111: 6299–6320.
49. Kihara Y, Maceyka M, Spiegel S, et al. Lysophospholipid receptor nomenclature review: IUPHAR Review 8. *Br J Pharmacol* 2014; 171: 3575–3594.
50. Paik J-H, Skoura A, Chae S-S, et al. Sphingosine 1-phosphate receptor regulation of N-cadherin mediates vascular stabilization. *Genes Dev* 2004; 18: 2392–2403.
51. Chiappini C, Tasciotti E, Fakhoury JR, et al. Tailored porous silicon microparticles: fabrication and properties. *Chemphyschem* 2010; 11: 1029–1035.
52. De Rosa E, Chiappini C, Fan D, et al. Agarose surface coating influences intracellular accumulation and enhances payload stability of a nano-delivery system. *Pharm Res* 2011; 28: 1520–1530.
53. Murphy CM and O'Brien FJ. Understanding the effect of mean pore size on cell activity in collagen-glycosaminoglycan scaffolds. *Cell Adh Migr* 2010; 4: 377–381.
54. Yeo Y and Park K. Control of encapsulation efficiency and initial burst in polymeric microparticle systems. *Arch Pharm Res* 2004; 27: 1–12.
55. Goranov AI, Cook M, Ricicova M, et al. The rate of cell growth is governed by cell cycle stage. *Genes Dev* 2009; 23: 1408–1422.
56. Curran J, Chen R and Hunt J. Controlling the phenotype and function of mesenchymal stem cells in vitro by adhesion to silane-modified clean glass surfaces. *Biomaterials* 2005; 26: 7057–7067.
57. Sunami H, Yokota I and Igarashi Y. Influence of the pattern size of micropatterned scaffolds on cell morphology, proliferation, migration and F-actin expression. *Biomater Sci* 2014; 2: 399–409.
58. Vasudev U, Kumar A and Menon B. Cell surface interactions in the study of biocompatibility. *Trends Biomater Artif Organs* 2002; 15: 37–41.
59. Collart-Dutilleul P-Y, Secret E, Panayotov I, et al. Adhesion and proliferation of human mesenchymal stem cells from dental pulp on porous silicon scaffolds. *ACS Appl Mater Interfaces* 2014; 6: 1719–1728.
60. Anselme K. Osteoblast adhesion on biomaterials. *Biomaterials* 2000; 21: 667–681.